

See discussions, stats, and author profiles for this publication at: <https://www.researchgate.net/publication/229897579>

# Optical Anisotropy of Tethered Chains

ARTICLE *in* MACROMOLECULES · OCTOBER 1992

Impact Factor: 5.8 · DOI: 10.1021/ma00047a013

---

CITATIONS

56

---

READS

21

## 2 AUTHORS, INCLUDING:



[Glenn H Fredrickson](#)

University of California, Santa Barbara

434 PUBLICATIONS 28,531 CITATIONS

[SEE PROFILE](#)

## Optical Anisotropy of Tethered Chains

Timothy P. Lodge\*

Department of Chemistry, University of Minnesota, Minneapolis, Minnesota 55455

Glenn H. Fredrickson

Department of Chemical & Nuclear Engineering, University of California,  
Santa Barbara, California 93106

Received May 11, 1992; Revised Manuscript Received July 6, 1992

**ABSTRACT:** The static intrinsic birefringence and dichroism of dense assemblies of tethered chains, or “brushes”, are computed. The classical trajectory analogy is used to calculate the average segmental anisotropy for strongly-stretched chains, as a function of distance from the grafting surface. This result is used to estimate the birefringence and dichroism of planar polymer brushes and strongly-segregated block copolymer lamellae and cylinders. The birefringence,  $\Delta n$ , varies as the ratio  $L^2/M\langle h^2 \rangle_0$ , where  $L$  is the layer thickness,  $M$  the chain length, and  $\langle h^2 \rangle_0$  the mean-square unperturbed end-to-end distance. Consequently,  $\Delta n$  is predicted to be independent of  $M$  for tethered chains where  $L \sim M$ ; however, for block copolymers in the strong-segregation limit,  $\Delta n \sim M^{-0.67}$ . For lamellar block copolymers, the calculations indicate that the intrinsic birefringence is surprisingly large and, for the most commonly-examined chemical systems, is often comparable to, or even greater than, the estimated form birefringence. This result reflects the *orientation* of the chains, i.e., the tendency of the block end-to-end vectors to be aligned, more than *stretching*. Calculations are also performed for labeled sections of a tethered chain, which indicate that it should be possible to assess the validity of the classical trajectory assumption via infrared dichroism measurements on appropriately deuterated samples.

### Introduction

A tethered polymer chain has one end confined to a point, a line, or a surface. Such confinement arises naturally in many polymer systems, including micelles, grafted layers, branched polymers, and block copolymer microstructures. Tethering leads to a variety of interesting physical properties, as has recently been discussed.<sup>1</sup> In addition to the loss of translational entropy, a consequence of anchoring multiple chains in close proximity is the tendency of each chain to orient and “stretch” its end-to-end vector along the normal to the grafting site. The orientation and stretching exist at equilibrium, as a direct consequence of the crowding of chains near the tethered ends. In general, a flexible chain with a finite end-to-end distance will be optically anisotropic, and increasing the end-to-end distance will increase the anisotropy. In a quiescent polymer liquid, all orientations of the end-to-end vectors are equally probable, and the material will be optically isotropic. However, when a collection of chains are appropriately tethered, a net orientation of the end-to-end vectors is possible, and a macroscopic optical anisotropy can result. This phenomenon is the subject of this paper.

The concentration profile and chain extension in a dense polymer brush, where the individual chains are strongly stretched, have been studied extensively. Alexander and de Gennes<sup>2</sup> first proposed a mean-field treatment of a polymer brush, in which the layer thickness,  $L$ , grows linearly with the molecular weight,  $M$ , the concentration profile is a step function, and the individual chains all have their free ends at the edge of the layer. Milner, Witten, and Cates<sup>3</sup> have presented an analytic self-consistent-field treatment of the brush, in the strong-stretching limit, which complements an earlier treatment of Semenov<sup>4</sup> for block copolymer microstructures. The resulting concentration profile is nearly parabolic rather than a step function, although the molecular weight scaling  $L \sim M$  is preserved. Furthermore, the conformation of

the average chain has been shown to follow the “classical trajectory” of a particle in a harmonic potential, and thus the stretching of each chain is not uniform along the chain but is strongest near the grafting site. Concomitantly, there was found to be a finite density of free (untethered) chain ends at all displacements through the layer.

Two experimentally-observable manifestations of molecular anisotropy are birefringence and dichroism, reflecting anisotropy in the polarizability and absorptivity, respectively. In this paper the optical anisotropy of a tethered chain is calculated using the classical trajectory approximation, combined with the appropriate free-end density profile. The chain is represented by  $N$  subchains, each with a root-mean-square end-to-end distance,  $b_0$ , and an optical anisotropy of the form derived for a Gaussian chain by Kuhn and Grün.<sup>5</sup> The resulting anisotropy per chain is then summed, to provide expressions for the birefringence and dichroism of (i) a polymer brush, both in the melt and in solution, (ii) a lamellar block copolymer microstructure, and (iii) a cylindrical block copolymer microstructure. The birefringence and dichroism thus calculated are static quantities, in the sense that no external field is applied. Furthermore, only the intrinsic, or “molecular”, contribution to the anisotropy of the material is calculated; form birefringence and form dichroism are not treated. Previously, it has been assumed that the form birefringence of a block copolymer microstructure would completely dominate the intrinsic contribution.<sup>6,7</sup> However, numerical estimates of the intrinsic birefringence show that, in general, this is not the case for a well-oriented (i.e., “single-crystal”) material. For the polystyrene-polydiene samples that have been studied,<sup>6,7</sup> the form contribution is relatively large, as it depends on the difference in the mean refractive index between the two blocks, whereas the intrinsic contribution is reduced, because the polarizability anisotropies differ in sign. Nevertheless, even in this case, the intrinsic and form contributions can be of comparable magnitude. Furthermore, this result does not depend on the individual chains being strongly stretched; the net orientation of the average

\* Author to whom correspondence should be addressed.

end-to-end vectors of the chains is sufficient to provide a substantial anisotropy.

The calculated optical anisotropy of a tethered chain differs by only about 25% when uniform stretching is assumed rather than the classical trajectory. Thus, given the inevitable uncertainties in the values of the necessary parameters, straightforward measurements of static birefringence or dichroism are unlikely to be able to distinguish between uniform and nonuniform stretching. However, if a suitable labeling technique is employed, it should be possible to assess the spatial variation in chain stretching. If selected sections of the tethered chains are labeled, for example by deuterium substitution in the case of infrared dichroism, such that only the anisotropy of the labeled segment contributes to the measurement, the results depend strongly on the assumed chain conformation. For the classical trajectory, the segmental anisotropy decreases steadily with distance from the grafting site, until it approaches zero for segments near the free end; conversely, for uniformly-stretched chains, the segmental anisotropy is independent of position along the chain.

## Theory

This section is divided into four parts. In the first, the anisotropy in the polarizability and absorptivity of a Gaussian chain is recalled, following the classical analysis of Kuhn and Grün.<sup>5</sup> The next part extends the calculation to a tethered chain comprising  $N$  subchains, following the classical trajectory analogy. Then, in the third section expressions for the birefringence and dichroism of polymer brushes, and lamellar and cylindrical block copolymer microstructures, are derived. Finally, calculations of the birefringence and dichroism from labeled segments of tethered chains are presented.

**A. Optical Properties of a Gaussian Subchain.** The polarizability tensor for a Gaussian chain was first derived by Kuhn and Grün.<sup>5</sup> For a chain made up of  $N_s$  links of length  $l$ , with polarizabilities  $\alpha_1$  along and  $\alpha_2$  normal to the link axis, respectively, the components of the average polarizability tensor for link  $s$  are given by

$$\langle \alpha_{ij} \rangle_s = \alpha_1 \langle u_{i,s} u_{j,s} \rangle + \alpha_2 \langle \delta_{ij} - u_{i,s} u_{j,s} \rangle \quad (1)$$

where  $u_{i,s} = l_{i,s}/l$ , with  $l_{i,s}$  the  $i$ th ( $i = x, y, z$ ) component of the end-to-end vector of link  $s$ ;  $\delta_{ij}$  is the Kronecker delta, and the brackets  $\langle \dots \rangle$  denote the appropriate conformational average. By assuming the links to be freely-jointed, and  $N_s$  large, Kuhn and Grün evaluated eq 1 for a chain with its end-to-end vector oriented along the  $z$  axis and obtained

$$\langle \alpha_{zz} \rangle_s = (1/3)(\alpha_1 + 2\alpha_2) + (2/5)(\alpha_1 - \alpha_2)(b^2/N_s l^2) \quad (2a)$$

$$\begin{aligned} \langle \alpha_{xx} \rangle_s &= \langle \alpha_{yy} \rangle_s = (1/3)(\alpha_1 + 2\alpha_2) - \\ &(1/5)(\alpha_1 - \alpha_2)(b^2/N_s l^2) \quad (2b) \end{aligned}$$

where  $b$  is the end-to-end distance. As in this instance  $\langle \alpha_{ij} \rangle_s$  is independent of  $s$ , the principal polarizabilities of the chain were simply obtained as

$$\gamma_1 = N_s \langle \alpha_{zz} \rangle_s = p + 2q(b^2/b_0^2) \quad (3a)$$

$$\gamma_2 = N_s \langle \alpha_{xx} \rangle_s = p - q(b^2/b_0^2) \quad (3b)$$

with  $p = (N_s/3)(\alpha_1 + 2\alpha_2)$  and  $q = (\alpha_1 - \alpha_2)/5$ ;  $b_0^2 = N_s l^2$ , the mean-square end-to-end distance of the chain (with an unconstrained end-to-end vector). In the calculation of the optical anisotropy of flexible chains, for example in the bead-spring model,<sup>8</sup> it is standard practice to assign

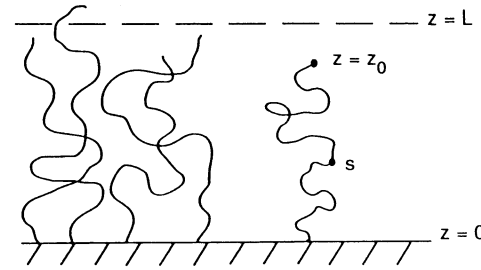


Figure 1. Schematic diagram of a brush of height  $L$ , with the individual polymer chains grafted at one end to a planar surface.  $s$  is the contour variable along the chain, and  $z_0$  is the spatial coordinate of the free end.

polarizabilities in the form of eqs 3a and 3b to each bead-spring unit, i.e., to each Gaussian subchain.

The dichroism associated with the same Gaussian chain can be computed by replacing  $\alpha_1$  and  $\alpha_2$  with  $\epsilon_1$  and  $\epsilon_2$ , respectively, defined as

$$\epsilon_1 = \epsilon \cos^2 \psi \quad (4a)$$

and

$$\epsilon_2 = (\epsilon/2) \sin^2 \psi \quad (4b)$$

where  $\epsilon$  is proportional to the extinction coefficient for the transition in question, and  $\psi$  is the angle between the transition dipole moment and the link axis (assuming a uniform distribution of transition moment orientations around the link axis). By analogy with eqs 3a and 3b, absorptivities parallel and perpendicular to the end-to-end vector of the chain may be expressed as

$$A_1 = (N_s/3)(\epsilon_1 + 2\epsilon_2) + (2/5)(\epsilon_1 - \epsilon_2)(b^2/b_0^2) \quad (5a)$$

$$A_2 = (N_s/3)(\epsilon_1 + 2\epsilon_2) - (1/5)(\epsilon_1 - \epsilon_2)(b^2/b_0^2) \quad (5b)$$

The dichroic ratio,  $A_1/A_2$ , and Hermann's orientation function,  $H = (A_1 - A_2)/(A_1 + 2A_2)$ , are then easily computed. In particular

$$H = (3/5)(1/N_s)(1/2)(3 \cos^2 \psi - 1)(b^2/b_0^2) \quad (6)$$

It is also common to express birefringence and dichroism in terms of the average second Legendre polynomial,  $\langle P_2(\cos \theta) \rangle = (1/2)[3 \langle \cos^2 \theta \rangle - 1]$ , where  $\theta$  is the angle between the chain backbone and the orientation direction; the relation between the two approaches will be explored subsequently.

**B. Optical Anisotropy of a Tethered Chain.** Consider a polymer layer, or brush, with thickness  $L$ . The brush consists of monodisperse, flexible chains, each made up of  $N$  subchains with average end-to-end distance  $b_0$ . Let one end of a given chain be tethered to a surface at  $z = 0$  and the other be located at a distance  $z_0$  from the surface, as shown in Figure 1. Interactions among the chains constrain the average end-to-end vector to lie along the  $z$  axis, yielding a net orientation of the chain, and in addition the chain may be stretched:  $z_0^2 \gtrsim Nb_0^2 = \langle h^2 \rangle_0$ . Both chain orientation and chain stretching contribute to a net optical anisotropy for each chain. (The terms "orientation" and "stretching" are distinct, in our usage. Orientation refers to the fact that the average end-to-end vector of a tethered chain always has a positive  $z$  component. Stretching refers to the distortion of the coil away from its unperturbed dimensions, in this case by increasing the average  $z$  component of the end-to-end distance. Thus, when the ratio  $z_0^2/\langle h^2 \rangle_0 \leq 1$ , in our terminology the chain is oriented but not stretched; when this ratio exceeds 1, the chain is both oriented and stretched.)

A straightforward approach to compute  $\gamma_{zz}$  and  $\gamma_{xx}$  would be to assume that each subchain is oriented and stretched by the same amount, i.e.,  $z_0 = Nb_z = Nb$ . The corresponding chain polarizabilities under this "uniform stretching" assumption would be

$$\gamma_{zz} = Np + 2qN(z_0^2/N^2)(1/b_0^2) = Np + 2q(z_0^2/\langle h^2 \rangle_0) \quad (7a)$$

$$\gamma_{xx} = Np - qN(z_0^2/N^2)(1/b_0^2) = Np - q(z_0^2/\langle h^2 \rangle_0) \quad (7b)$$

The polarizability tensor for the entire brush would be computed by integrating eqs 7a and 7b over the distribution of end-to-end distances and then multiplying by the number of chains. In the simplest approximation, such as in the Alexander-de Gennes brush,<sup>2</sup>  $z_0 = L$  for all chains. However, more detailed analysis predicts that the stretching is not uniform along the chain and that therefore eqs 7a and 7b are only approximate. Furthermore, the resulting parabolic concentration profile within the brush requires that a significant number of chain ends lie within the brush.

The local degree of stretching along the chain can be obtained by the classical trajectory argument, whereby the average path of the chain in the  $z$  direction, in the potential created by the neighboring chains, is equivalent to the trajectory of a particle in a harmonic potential.<sup>3,4</sup> This trajectory may be parametrized as

$$z = z_0 \sin(\pi s/2N) \quad (8)$$

and the local stretching is

$$\partial z / \partial s = (\pi z_0 / 2N) \cos(\pi s / 2N) \quad (9)$$

At this stage it is convenient to proceed in the continuum limit, so that the link index,  $s$ , becomes a continuous variable along the chain contour,  $0 \leq s \leq N$ , with  $s = 0$  corresponding to the tethered end. The trajectory is normalized by

$$\int_0^{z_0} (\partial s / \partial z) dz = N \quad (10)$$

Equation 9 also satisfies the boundary conditions that the stretching,  $\partial z / \partial s$ , vanishes at the free end and is maximized at the tethering surface. The continuous variable  $u_z^s$ , representing the  $z$  component of the unit tangent to the chain at contour position  $s$ , may be defined as

$$u_z^s \equiv (\sqrt{3}/b_0)(\partial z / \partial s) \quad (11)$$

and the average polarizabilities at position  $s$  are given by

$$\langle \gamma_{zz} \rangle_s = p + (2/3)q \langle u_z^s u_z^s \rangle \quad (12a)$$

$$\langle \gamma_{xx} \rangle_s = p - (1/3)q \langle u_z^s u_z^s \rangle \quad (12b)$$

From eq 9 it can be seen that  $u_z^s$  depends on  $z_0$ , and thus

$$\langle u_z^s u_z^s \rangle = \int_0^L g(z_0) (u_z^s)^2 dz_0 \quad (13)$$

where  $g(z_0) dz_0$  is the fraction of chains with free ends lying between  $z_0$  and  $z_0 + dz_0$ . Expressions for  $g(z_0)$  for strongly-stretched chains tethered to planar, cylindrical, and spherical surfaces have been given by Semenov<sup>4</sup> for the melt case and by Milner, Witten, and Cates<sup>3</sup> for a brush tethered to a planar surface in solution. The final expressions for the components of the average polarizability tensor for the entire chain are obtained as

$$\gamma_{zz} = \int_0^N \langle \gamma_{zz} \rangle_s ds \quad (14a)$$

$$\gamma_{xx} = \int_0^N \langle \gamma_{xx} \rangle_s ds \quad (14b)$$

By symmetry, the remaining elements of the polarizability tensor are simply evaluated as  $\gamma_{yy} = \gamma_{xx}$ ,  $\gamma_{xy} = \gamma_{xz} = \gamma_{yz} = 0$ .

**C. Birefringence and Dichroism of Assemblies of Tethered Chains.** The birefringence of a dense polymer system may be calculated as<sup>9</sup>

$$\Delta n = (2\pi/9n)(n^2 + 2)^2(cN_a/M)\Delta\gamma \quad (15)$$

where  $n$  is the mean refractive index of the medium,  $c$  is the concentration,  $N_a$  is Avogadro's number,  $M$  is the chain molecular weight, and  $\Delta\gamma = \gamma_{zz} - \gamma_{xx}$ . The factor  $cN_a/M$  accounts for the number of chains per unit volume. Equation 15 rests on the application of the Lorentz-Lorenz equation and thus assumes that the internal electric field at a given subchain, due to the presence of neighboring subchains, is isotropic and homogeneous throughout the sample. This assumption may not be strictly valid for highly-oriented samples or near the surfaces of the sample. However, although tethered chains can be stretched significantly relative to their unperturbed dimensions, they are not so strongly stretched that  $L$  approaches  $Nb_0$ . The role of the interface is likely to be diminished in block copolymer microstructures, because the interface is not sharp and because the mean refractive indices of the components are usually not too different. Thus, in general, one may expect eq 15 to be a reasonable approximation.

**(i) Polymer Brush.** For a polymer brush tethered to a flat surface, the concentration profile is very close to parabolic, with  $c(z) \sim z^2 - L^2$ . The distribution of free ends in the melt case has been given by Semenov<sup>4</sup> and may be written as

$$g(z_0) = (1/L)(z_0/L)(1 - z_0^2/L^2)^{-0.5} \quad (16)$$

where the normalization condition

$$\int_0^L g(z_0) dz_0 = 1 \quad (17)$$

has been applied. From eqs 9 to 14, the polarizability anisotropy per chain may be calculated as

$$\Delta\gamma = 3q(\pi^2/12)(L^2/\langle h^2 \rangle_0) \quad (18)$$

and the birefringence of the brush as

$$\Delta n = (\pi^3/90)(\alpha_1 - \alpha_2)[(n^2 + 2)^2/n](cN_a/M)(L^2/\langle h^2 \rangle_0) \quad (19)$$

For comparison, if uniform stretching had been assumed, as in eqs 7a and 7b, but using the same  $g(z_0)$ , the numerical front factor would have been  $8\pi/90$ , a reduction in the birefringence of only 23%. However, this particular functional form for  $g(z_0)$  is predicated on a parabolic pressure field in a melt brush, which requires nonuniform stretching for self-consistency. A more appropriate comparison, therefore, would be to the Alexander-de Gennes step-profile brush,<sup>2</sup> where uniform stretching is required. Then the numerical prefactor in eq 19 would become  $2\pi/15$ , an increase of approximately 22% (i.e., the factor of  $\pi^2/12$  in eq 18 would be removed). Thus, the total anisotropy of each chain in the brush is only weakly dependent on the assumed average chain trajectory. In contrast, however, if the chains are labeled at various locations along the chain, the results depend very much on the local degree of stretching, as will be discussed in section D. Finally, Hermann's orientation function for

each chain in the melt brush is given by

$$H = (A_{zz} - A_{xx})(A_{zz} + 2A_{xx}) \\ = (\pi^2/20)(1/2)(3\cos^2 \psi - 1)(1/N_s N)(L^2/\langle h^2 \rangle_0) \quad (20)$$

For a brush in a good solvent, the expression for  $g(z_0)$  corresponding to eq 16 is<sup>3</sup>

$$g(z_0) = (1/L)(z_0/L)(1 - z_0^2/L^2)^{0.5} \quad (21)$$

The principal difference between eqs 16 and 21 is that, in the former, the free-end density has an integrable singularity at the edge of the brush, whereas, in the latter, it exhibits a maximum at a finite  $z < L$ . The reason for this difference is that, in the solution case, the constraint of constant density is relaxed by the presence of solvent. Analysis entirely analogous to that leading to eq 19 gives the following expression for the birefringence of a brush in a good solvent:

$$\Delta n = (\pi^3/150)(\alpha_1 - \alpha_2)[(n^2 + 2)^2/n](cN_a/M)(L^2/\langle h^2 \rangle_0) \quad (22)$$

The numerical prefactor is reduced by a factor of  $3/5$  from the melt case, reflecting the shorter average end-to-end distance in the solvated brush. From eqs 19 and 22, it is clear that the optical anisotropy of the brush depends primarily on the degree of stretching, quantified by the ratio  $L^2/\langle h^2 \rangle_0$ . For a dense, solvated brush

$$L \sim (N/g)\xi = Nb(b/\xi)^{(1-\nu)/\nu} \quad (23a)$$

where  $\nu = 0.6$  in a good solvent and 0.5 in a  $\theta$  solvent;  $g$  is the number of subchains in a blob, and  $\xi$  is the blob size. The blob size in this picture is determined by the surface grafting density,  $\sigma$ , as  $\xi \sim \sigma^{-0.5}$ . For the melt brush

$$L \sim Nb^3\sigma \quad (23b)$$

In both the melt and solvated cases, the birefringence per chain increases as  $N$ , whereas the birefringence per unit volume of the brush is independent of  $N$ . The latter result is a consequence of the fact that, although the chain stretching increases as  $N$ , the average anisotropy per subchain is independent of  $N$ . Hermann's orientation function per chain is independent of  $N$  and decreases as  $1/N$  per unit volume of the brush.

**(ii) Block Copolymer Lamellae.** For a block copolymer in the strong segregation limit (SSL),  $L \sim N^{0.67}$ .<sup>4,10</sup> Thus, the individual blocks are stretched away from the interfaces between microdomains, but the stretching is weaker than in the brush case. The primary reason for this difference is the fact that the block copolymers can adjust their tethering density at the interface, to lessen the entropic penalty associated with stretching. Nevertheless, the birefringence of a lamellar phase can be estimated by using the same approach as for the melt brush. The result is

$$\Delta n = (\pi^3/90)N_a[(M_A/\rho_A) + (M_B/\rho_B)]^{-1}\{[(n_A^2 + 2)^2/n_A](\alpha_1 - \alpha_2)_A(L_A^2/\langle h_A^2 \rangle_0) + [(n_B^2 + 2)^2/n_B](\alpha_1 - \alpha_2)_B(L_B^2/\langle h_B^2 \rangle_0)\} \quad (24)$$

where the subscripts A and B denote the properties of the respective blocks. Thus,  $\rho_A$  is the mass density of block A in the A microdomain, and  $L_A$  is the half-thickness of the A microdomain. The overall period of the lamellar structure is therefore  $2(L_A + L_B)$ , and the number of A chains is constrained to be equal to the number of B chains, i.e.

$$\rho_A L_A/M_A = \rho_B L_B/M_B \quad (25)$$

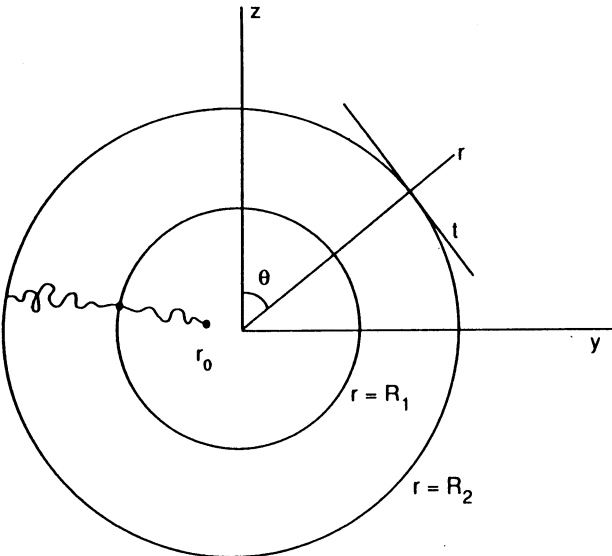


Figure 2. Schematic diagram of a cylindrical block copolymer morphology. The block in the inner cylinder has its free end at  $r_0$ , while the free end of the block in the outer layer is assumed to lie on the outer surface,  $r = R_2$ . The Cartesian coordinate system ( $r, t$ ) forms an angle  $\theta$  with the laboratory ( $y, z$ ) frame.

Thus the birefringence *per chain* grows as  $N^{0.33}$ , but the birefringence of the *sample* decreases as  $N^{-0.67}$ . The relative contributions of the two blocks are fixed by the relative refractive indices, segmental anisotropies, and block stretching. As lamellar phases are obtained for nearly symmetrical block copolymers in the SSL, the relative stretching of the two blocks should be comparable. Numerical estimates of  $\Delta n$  will be given in the Discussion.

**(iii) Block Copolymer Cylinders.** For AB diblock and ABA triblock copolymers in which the volume fraction of A lies between approximately 0.15 and 0.35, the SSL morphology is a hexagonal array of cylinders. The birefringence of such an array may be calculated by the approach given above, albeit with some modifications due to the curvature of the interface. Let the inner cylinder have radius  $R_1$  and contain the A blocks, and let the average thickness of the B layer be  $R_2 - R_1$ , as shown in Figure 2. Although the B domains must be distorted slightly from a cylindrical annulus in order to fill space in the hexagonal array, this effect will be ignored here. The calculation of the chain anisotropy is performed first in the ( $r, t, x$ ) Cartesian coordinate system, where  $r$  is the radial (stretching) direction, the cylinder axis lies along  $x$ , and  $t$  is the tangential direction orthogonal to  $r$  and  $x$ . The  $r$  and  $t$  axes form an angle  $\theta$  with the  $z$  and  $y$  laboratory axes, respectively. The result is then transformed to the ( $x, y, z$ ) laboratory frame and averaged over  $\theta$ , to compute the net birefringence.

The nonzero elements of the polarizability tensor of the Gaussian subchain are given by

$$\langle \gamma_{zz} \rangle_s = p + (q/3)[2 \cos^2 \theta - \sin^2 \theta] \langle u_r^s u_r^s \rangle \quad (26a)$$

$$\langle \gamma_{yy} \rangle_s = p + (q/3)[2 \sin^2 \theta - \cos^2 \theta] \langle u_r^s u_r^s \rangle \quad (26b)$$

$$\langle \gamma_{xx} \rangle_s = p - (q/3) \langle u_r^s u_r^s \rangle \quad (26c)$$

$$\langle \gamma_{zy} \rangle_s = \langle \gamma_{yz} \rangle_s = q[\cos \theta \sin \theta] \langle u_r^s u_t^s \rangle \quad (26d)$$

The use of a Cartesian coordinate system for the subchain is, in fact, tantamount to assuming that the  $x$  and  $t$  components of each subchain are the same. Physically, this corresponds to assuming that each chain senses only

one preferred direction,  $r$ , and that the average trajectories of a chain in the other two directions are equivalent.

For a chain confined to the inner cylinder, Semenov found

$$g(r_0) = (2/R_1)(r_0/R_1) \tanh^{-1} [1 - (r_0/R_1)^2]^{0.5} \quad (27)$$

where  $r_0$  is the radial position of the free end; as in the planar case, the normalization of  $g(r_0)$  differs slightly from that given by Semenov, in order that

$$\int_0^{R_1} g(r_0) dr_0 = 1 \quad (28)$$

Use of eq 27 leads to

$$(1/3)\langle u_r u_r \rangle = (13\pi^2/96)(R_1^2/\langle h^2 \rangle_0) \quad (29)$$

To find the average polarizability per chain in the cylinder, it is necessary to average over  $0 \leq \theta \leq 2\pi$ , whereby the terms containing  $\cos^2 \theta$  and  $\sin^2 \theta$  in eqs 26a and 26b amount to a factor of  $1/2$ , eq 26c is unchanged, and the off-diagonal elements in eq 26d vanish. Finally

$$\Delta\gamma = \gamma_{zz} - \gamma_{xx} = (13\pi^2/320)(\alpha_1 - \alpha_2)(R_1^2/\langle h^2 \rangle_0) \quad (30)$$

This quantity is a factor of  $13/16$  less than that for a chain tethered to a planar surface.

The average conformation of a chain in the outer cylinder must be treated in a different way. Due to the convexity of the tethering surface, the distribution of free ends would have negative values in a region close to the surface, if the classical trajectory were employed. The exact solution to this problem is rather complicated, but the Alexander-de Gennes ansatz, namely, that all of the chains extend to  $r = R_2$ , provides an excellent approximation to the free energy.<sup>11</sup> In this case, the relevant quantity,  $\partial r/\partial s$ , is obtained by invoking incompressibility. An annulus of cross-sectional area  $2\pi r dr$  and length  $l$  must occupy a volume  $vQ ds$ , where  $v$  is the segment volume and  $Q$  is the number of chains in the cylinder of length  $l$ ; thus

$$\partial r/\partial s = vQ/2\pi rl \quad (31)$$

The condition

$$\int_{R_1}^{R_2} dr 2\pi lr = \int_0^N ds vQ \quad (32)$$

establishes that

$$\partial r/\partial s = (R_2^2 - R_1^2)/2rN \quad (33)$$

and so

$$(1/3)\langle u_r^s u_r^s \rangle = ((R_2^2 - R_1^2)/2rNb_0)^2 \quad (34)$$

This expression may be inserted into eqs 26a-d and then integrated over the chain to arrive at expressions analogous to eq 29. To perform this step, it is helpful to note that

$$\begin{aligned} \int_0^N ds \langle u_r^s u_r^s \rangle &= \int_{R_1}^{R_2} dr (\partial s/\partial r) \langle u_r^s u_r^s \rangle = \\ &\int_{R_1}^{R_2} dr (1/b_0^2)(\partial r/\partial s) = (R_2^2 - R_1^2)(1/2Nb_0^2) \ln(R_2/R_1) \end{aligned} \quad (35)$$

The final expression for the average polarizability anisotropy of a chain in the outer cylinder, in the  $(x, y, z)$  coordinate system, becomes

$$\Delta\gamma = (3/20)(\alpha_1 - \alpha_2) \ln(R_2/R_1)[(R_2 + R_1)/(R_2 - R_1)][(R_2 - R_1)^2/\langle h^2 \rangle_0] \quad (36)$$

In eq 36, the factor  $(R_2 + R_1)/(R_2 - R_1)$  arises in order that the chain stretching be expressed as  $(R_2 - R_1)^2/\langle h^2 \rangle_0$ , to correspond to the form in eqs 19, 24, and 30. The numerical prefactor in eq 36, corresponding to  $13\pi^2/320$  in eq 30 for

a chain in the inner cylinder, depends on  $R_2/R_1$ . However, this ratio does not vary much for block copolymers, and a typical value is approximately 2. In this case the numerical prefactor becomes 0.31, compared to 0.40 for the inner cylinder.

Equations 30 and 36 permit a general expression for the intrinsic contribution to the birefringence of a regular array of block copolymer cylinders to be developed. The analysis proceeds exactly as for the lamellar case, under the constraint that

$$(\rho_A/M_A)R_1^2 = (\rho_B/M_B)(R_2^2 - R_1^2) \quad (37)$$

The final result is

$$\Delta n = (13\pi^3/1440)N_a[(M_A/\rho_A) + (M_B/\rho_B)]^{-1}\{\Gamma_A + \Gamma_B\} \quad (38a)$$

with

$$\Gamma_A = [(n_A^2 + 2)^2/n_A](\alpha_1 - \alpha_2)_A(R_1^2/\langle h^2 \rangle_0) \quad (38b)$$

and

$$\Gamma_B = [(n_B^2 + 2)^2/n_B](\alpha_1 - \alpha_2)_B(48/13\pi^2) \ln(R_2/R_1)[(R_2 + R_1)/(R_2 - R_1)][(R_2 - R_1)^2/\langle h^2 \rangle_0] \quad (38c)$$

**D. Labeled Segments of a Tethered Chain.** As mentioned in the Introduction, the anisotropy of a labeled section of a tethered chain could provide a means to assess the accuracy of the classical trajectory approach. Consider a tethered chain of length  $N$ , with a labeled section running from contour index  $s_1$  to index  $s_2$ ,  $0 \leq s_1 \leq s_2 \leq N$ . For simplicity, only the case of a planar grafting surface is considered. The analysis proceeds exactly as in sections B and C, except that the optical factor  $q$  becomes a function of  $s$ . For a labeled segment running from  $s_1$  to  $s_2$ ,  $q(s) = q$  within the segment and  $q = 0$  outside the segment. The more general case of a multiblock copolymer may also be considered; a similar approach has been taken in calculating the oscillatory flow birefringence properties of block copolymers following Rouse-Zimm<sup>12</sup> or Doi-Edwards<sup>13</sup> dynamics. For the anisotropic part of  $\gamma_{zz}$ , the integration over the chain contour variable leads to the proportionality

$$\gamma_{zz}(s_1, s_2) \sim \int_{s_1}^{s_2} \cos^2(\pi s/2N) ds = (1/2)(s_2 - s_1) + (N/2\pi)[\sin(\pi s_2/N) - \sin(\pi s_1/N)] \quad (39)$$

Thus, the birefringence attributable to the labeled segment will be

$$\Delta n(s_1, s_2) \sim \gamma_{zz}(s_1, s_2) \quad (40)$$

The corresponding integral for the entire chain ( $s_1 = 0, s_2 = N$ ) gives a factor of  $N/2$ , and so the relative birefringence due to the labeled segment may be expressed as

$$\Delta n(f_1, f_2)/\Delta n_0 = (f_2 - f_1) + (1/\pi)[\sin(\pi f_2) - \sin(\pi f_1)] \quad (41)$$

where  $f_1 = s_1/N$  and  $f_2 = s_2/N$  are the fractional positions along the chain. As a specific example, consider a labeled segment equal in length to one-fifth of the chain. If  $f_1 = 0$ , corresponding to the labeled segment at the tethered end, the relative birefringence would be 0.387. For a segment in the middle, i.e.,  $f_1 = 0.4, f_2 = 0.6$ , the relative birefringence would be 0.2, whereas for the segment at the free end, the contribution would be 0.013. In contrast, for the uniformly stretched chain, the relative birefringence would be 0.2, independent of position. The results indicate that the anisotropy of a tethered chain following the classical trajectory tends to zero toward the free end.

**Table I**  
**Relative Optical Anisotropy for Tethered Chains in Different Geometries**

geometry	$g(z_0)$	numerical prefactor in eq 18
step function		
(mean-field) brush	$\delta(z_0 - L)$	1
melt SCF brush	$(z_0/L^2)[1 - (z_0/L)^2]^{-0.5}$	$\pi^2/12$
solution SCF brush	$(z_0/L^2)[1 - (z_0/L)^2]^{0.5}$	$\pi^2/20$
inner cylinder, SSL	$(2r_0/R_1^2) \tanh^{-1} [1 - (r_0/R_1)^2]^{0.5}$	$13\pi^2/192$
outer cylinder, SSL	$\delta(z_0 - R_2)$	$(1/4)[(R_2 + R_1)/(R_2 - R_1)] \ln (R_2/R_1)$

It would be experimentally more convenient to test this proposition with infrared dichroism and deuterium-labeled chain segments. Indeed, styrene-isoprene block copolymers with perdeuterated styrene segments adjacent to the isoprene junction, and at the free styrene end, have been prepared.<sup>14</sup> By selecting an appropriate wavelength, it is possible to make  $\epsilon = 0$  for either the deuterated or the protonated sections. In contrast, it is virtually impossible to make  $(\alpha_1 - \alpha_2) = 0$  for a polymer, and certainly not by isotopic substitution. The relative Hermann's orientation function for a labeled segment is

$$H(f_1, f_2)/H_0 = 1 + (1/\pi)(f_2 - f_1)^{-1}[\sin(\pi f_2) - \sin(\pi f_1)] \quad (42)$$

For the three locations of the labeled fifth of the chain considered above, the corresponding values of  $H(f_1, f_2)/H_0$  would be 1.935, 1, and 0.065. In particular, the difference in  $H$  between the two extreme locations of the labeled segment is a factor of 30. However, it must be emphasized that this is a relative value of  $H$ ; the values determined for the labeled and unlabeled chains could both be very small, due to the factor of  $1/N_s N$  in the isotropic contribution (see eq 20).

## Discussion

The optical anisotropy of tethered chains has been computed for five different situations, corresponding to (i) the Alexander-de Gennes step-profile planar brush, (ii) the self-consistent-field parabolic brush in the melt, (iii) the self-consistent-field parabolic brush in solution, (iv) the self-consistent-field brush tethered to the inside of a cylindrical surface, and (v) a step-profile melt brush tethered to the outside of a cylindrical surface. In each case, the birefringence of the brush varies as  $(1/M)(\alpha_1 - \alpha_2)(L^2/\langle h^2 \rangle_0)$ , where  $L$  is the brush height and  $\langle h^2 \rangle_0$  is the mean-square end-to-end distance of the unperturbed chain. The numerical prefactors vary from case to case, due to differences in geometry and the distribution of free ends; these differences are summarized in Table I. For the melt case, the birefringence magnitude decreases as (i) > (ii) > (iv) > (v), a sequence which is straightforward to understand; numerically, the differences are not great.

The applicability of the strong-stretching assumption and the classical trajectory to strongly-segregated block copolymer lamellae and cylinders is possibly questionable; in general,  $L^2/\langle h^2 \rangle_0$  is of order 1 for most block copolymer microstructures (vide infra). However, alternative, analytical expressions for  $g(z_0)$  in block copolymer microstructures are not yet available, although numerical estimates could be obtained.<sup>15</sup> Presumably, the real situation lies between the limits where the free ends all lie at  $z = L$  and where the free ends are uniformly distributed throughout the microdomain; the latter situation appears less probable. The strong-stretching assumption employed here gives a numerical factor of  $\pi^2/$

12, whereas the two limits would give 1 and  $1/4$ , respectively; thus, the final result is certainly plausible. It should also be recalled that the interface between the microdomains has been assumed to be infinitely sharp.

The Gaussian chain result of Kuhn and Grün might appear to be inapplicable to the segments of tethered chains; however, this is, in fact, not a restrictive assumption. First, the Gaussian assumption only leads to the factor  $(3/5)(\alpha_1 - \alpha_2)$  in  $\Delta\gamma$  given by eqs 3a and 3b; the proportionality to  $b^2/b_0^2$  is inherent to an experiment that senses  $\langle P_2(\cos \theta) \rangle$ . Second, there is always some ambiguity in the value of the segmental anisotropy. Yet, the use of the Kuhn and Grün approach permits direct connection with a large body of data on the stress-optic coefficient, whereby values of  $\alpha_1 - \alpha_2$  may be obtained independently (vide infra). Third, it seems more reasonable to apply the classical trajectory analogy to the subchains of each tethered chain rather than to the monomers themselves, and thus an expression for the subchain anisotropy is required in any case. However, as mentioned previously it is possible to re-express the results obtained here in terms of  $\langle P_2(\cos \theta) \rangle$ , as follows.

For the Gaussian chain considered by Kuhn and Grün

$$\langle P_2(\cos \theta) \rangle = (3/5)(1/N_s)(b^2/b_0^2) \quad (43)$$

Our subsequent analysis proceeded by replacing  $b^2/b_0^2$  with  $(1/3)\langle u_z s u_z s \rangle$ . Thus, if  $\langle P_2(\cos \theta) \rangle$  is used to replace the right-hand side of eq 43 in, for example, eqs 3 and 5, the results can be obtained in terms of  $\langle P_2(\cos \theta) \rangle$  and independent of any Gaussian assumption;  $\cos \theta$  and  $\alpha_1 - \alpha_2$  could be interpreted as referring to the actual monomer units. For some polymers, such as polystyrene, explicit calculations of the birefringence in terms of bond angles and bond polarizabilities have been performed,<sup>16,17</sup> and these expressions may be used if desired.

Considerable progress has been made in the preparation of ordered assemblies of tethered chains, both by adsorption or grafting to a surface and by macroscopic orientation of block copolymer microstructures; thus, it should be possible to investigate these predictions experimentally. For brushes, several computer simulations have been reported<sup>18-23</sup> and one recent experimental study.<sup>24</sup> For block copolymers, Folkes and Keller reported static birefringence measurements on well-ordered lamellar and cylindrical samples some years ago.<sup>6,7</sup> More recently, at least three groups have examined the birefringence of block copolymers near the ordering transition.<sup>25-27</sup>

A variety of computer simulations of adsorbed polymer chains in general, and end-anchored chains in particular, have been undertaken.<sup>18-23</sup> Understandably, the primary focus has been on the concentration profile within the brush and the  $M$  scaling of  $L$ . In general, the concentration profiles emerging from the simulations are consistent with the parabolic form, when the grafting density is sufficiently high. However, in at least three studies some attention was paid to the determination of the free-end density,  $g(z_0)$ , and to the average chain orientation as a function of  $z$ . Murat and Grest used molecular dynamics to examine a solvated brush attached to a planar surface<sup>19</sup> and subsequently to the outside of a cylindrical surface.<sup>21</sup> In the former case, at sufficiently high grafting density the concentration profile was parabolic, and  $g(z_0)$  exhibited a maximum which moved away from the surface as the grafting density increased. Concurrently, the  $z$  dependence of the local degree of chain orientation was consistent with the classical trajectory. For cylindrical surfaces, the results were in less good agreement with the self-consistent-field model. In particular, there appeared to be no evidence of a "dead zone" near the surface, where  $g(z_0)$  vanishes.

However, the simulation was for a cylindrical brush immersed in a good solvent, whereas we have only considered the melt cylindrical brush case here. Recently, Lai and Binder used the bond fluctuation Monte Carlo algorithm to examine chains tethered to a planar surface, in a good solvent.<sup>22</sup> In this case the results for the local stretching were in excellent agreement with the classical trajectory. From these simulations, therefore, it seems quite reasonable to adopt the classical trajectory approximation, provided that the chains are sufficiently stretched.

Waldman et al.<sup>24</sup> have succeeded in measuring the dichroism of a brush comprising polystyrene chains anchored to a gold substrate via sulfur functionalities at the end of the chain. The quantitative analysis is somewhat hindered by the surface selection rule which prohibits measurement of the absorptivity parallel to the surface. However, the results are clearly indicative of a strong chain orientation normal to the surface.

Folkes and Keller reported extensive characterization of the morphology of lamellar and cylindrical polystyrene-polybutadiene block copolymers, using electron microscopy and X-ray scattering in addition to static birefringence.<sup>6,7</sup> The optical results were interpreted primarily in terms of the form birefringence contribution, and it is therefore of interest to estimate the intrinsic birefringence for these samples. The lamellar sample was a poly(styrene-butadiene-styrene) triblock, with molecular weights of  $1.4 \times 10^4$  for each styrene block and  $3.0 \times 10^4$  for the central butadiene block. Care was taken to generate a single-crystal sample, and the measured birefringence was  $(-2.7 \pm 0.2) \times 10^{-3}$ , relative to the lamellar normal (the  $z$  axis in our nomenclature). The form birefringence was estimated using an expression derived for an alternating stack of slabs of two materials, with refractive indices  $n_A$  and  $n_B$  and volume fractions  $\phi_A$  and  $\phi_B$ .<sup>9</sup>

$$\Delta n_f = (n_A n_B) / [\phi_A n_B^2 + \phi_B n_A^2]^{0.5} - ([\phi_A n_A^2 + \phi_B n_B^2]^{0.5}) \quad (44)$$

This expression assumes that the wavelength of the light is much larger than the dimensions of the slabs and that the interfaces between the slabs are sharp. The former assumption is reasonable, given a measured periodicity of 26 nm. The latter assumption is more questionable, given an interfacial zone of about 2 nm for styrene-diene block copolymers,<sup>28</sup> as there are two interfaces per period, approximately 15% of the material has a mean refractive index between those of the bulk polymers, which will reduce  $\Delta n_f$ . Using values for  $n_{PS}$  and  $n_{PB}$  of 1.59 and 1.52, respectively, and  $\phi_{PS} = 0.43$ , a value of  $\Delta n_f = -1.54 \times 10^{-3}$  was calculated. Thus, Folkes and Keller inferred an intrinsic birefringence of  $-1.16 \times 10^{-3}$  for this particular sample. In addition, they were able to conclude from infrared dichroism measurements that the polystyrene chains were oriented normal to the interface and possibly extended by approximately 10%; dichroic signals from the polybutadiene chains were too small to be interpreted.

To compute the intrinsic contribution,  $\Delta n_i$ , to the birefringence of this sample via eq 24, we make the assumption that the morphology and the chain conformations are equivalent to those for a styrene-butadiene diblock with  $M_{PS} = 1.4 \times 10^4$  and  $M_{PB} = 1.5 \times 10^4$ . The polarizability anisotropy,  $\alpha_1 - \alpha_2$ , may be estimated as  $-1.5 \times 10^{-23} \text{ cm}^3$  for PS and  $3 \times 10^{-24} \text{ cm}^3$  for PB,<sup>29</sup> and the corresponding densities are 1.05 and  $0.895 \text{ g/cm}^3$ , respectively. If we make the further assumption that the stretching is identical in the two blocks, the result is

$$\Delta n_i = -1.1 \times 10^{-3} (L^2 / \langle h^2 \rangle_0) \quad (45)$$

which is in close agreement to the measured value, for

little or no stretching ( $L^2 / \langle h^2 \rangle_0 \approx 1$ ). To assess whether this result is reasonable,  $L^2 / \langle h^2 \rangle_0$  may be estimated directly. Folkes and Keller reported that the lamellar period was roughly equal for the two blocks, and thus  $2L \approx 13 \text{ nm}$  and  $L^2 \approx 42 \text{ nm}^2$ . For PS, the unperturbed dimensions may be estimated as  $\langle h^2 \rangle_0 = 6R_g^2 \approx 6(0.00087M) \text{ nm}^2$ , yielding a value of  $73 \text{ nm}^2$  for this sample. This calculation suggests that the chains are not stretched in the  $z$  direction but merely oriented. For PB,  $\langle h^2 \rangle_0 \approx 0.0088M \text{ nm}^2$ , corresponding to  $132 \text{ nm}^2$ . Thus, the stretching ratios are 0.57 for the PS block and 0.32 for the PB block; using these numbers, a value for  $\Delta n_i$  of  $-7 \times 10^{-4}$  would be obtained.

The cylindrical sample examined by Folkes and Keller was a styrene-butadiene-styrene triblock with  $M_{PS} = 1.0 \times 10^4$  for each block and  $M_{PB} = 5.5 \times 10^4$ . The PS cylinder radius,  $R_1$ , was determined to be 7.5 nm and  $R_2 = 2R_1$ . The static birefringence was measured as  $4.9 \times 10^{-4}$ . The form birefringence contribution was estimated by the expression<sup>30</sup>

$$\Delta n_f = [\phi_A n_A^2 + \phi_B n_B^2]^{0.5} - n_B \{[(1 + \phi_A)n_A^2 + \phi_B n_B^2]/[(1 + \phi_A)n_B^2 + \phi_B n_A^2]\}^{0.5} \quad (46)$$

to be  $5.2 \times 10^{-4}$ , using  $\phi_A = 0.2$  and the refractive indices given above. This implies an intrinsic birefringence contribution of  $-3 \times 10^{-5}$ . Using the same parameter values as before, the stretching ratios for the PS and PB blocks are estimated to be 1.1 and 0.23, respectively, thus indicating that the conformations of the chains in the inner cylinders are considerably more distorted, as expected, although the magnitude of the difference is quite large. However, even in the lamellar case the PB chains were less extended than the PS blocks. Equations 36a-c predict an intrinsic birefringence of  $+8.7 \times 10^{-4}$ , which is larger than both the measured birefringence and the estimated form contribution. Note that  $\Delta n_i$  is positive in sign because  $\Delta n_f$  is computed relative to the cylinder axis (the  $x$  axis in our nomenclature). The origins of this discrepancy are not immediately clear. However, it is too large to be ascribed solely to the assumed chain trajectories; use of the uniform stretching assumption would reduce the predicted birefringence of the PS block (which presumably dominates the net intrinsic birefringence) by only a few percent. One possibility is that the PB chains are more greatly extended than the above calculation indicates, due to the triblock nature of the chain; some PS end blocks might be located in non-nearest-neighbor cylinders. A larger contribution from the butadiene phase would reduce the net birefringence.

Two groups have used the measurement of static birefringence to detect the microphase-separation transition, in PS-PMMA melts<sup>25</sup> and in PS-PI solutions.<sup>26</sup> In both cases, however, the ordered samples were "polycrystalline", so a quantitative determination of the birefringence was not possible. The calculations presented here suggest that, in both cases, the resulting signals reflect a mixture of form and intrinsic birefringence, with the former providing the larger contribution. Of course, in the vicinity of the ordering transition, the system will not be in the strong-segregation limit, and neither our expression for  $\Delta n_i$  nor the classical result  $\Delta n_f$  will be quantitatively applicable. Chin et al. used an optical waveguide technique to determine the birefringence of PS-PMMA lamellae on a gold substrate;<sup>27</sup> the result was  $\Delta n = (-2.0 \pm 0.2) \times 10^{-3}$ . The authors estimate  $\Delta n_f$  to be  $-3.6 \times 10^{-3}$ , via eq 44, which is likely to be an overestimate due to the interfacial regions, as they point out. From the reported lamellar spacings, we estimate  $L^2 / \langle h^2 \rangle_0$  to be 0.4 and  $\Delta n_i$  to be  $-1.6 \times 10^{-4}$ , via eq 24. Thus, these results appear to be

**Table II**  
**Estimated Intrinsic and Form Birefringence for Lamellar Block Copolymers**

polymer	<i>n</i>	$(\alpha_1 - \alpha_2)$ , cm <sup>3</sup>
polystyrene (PS)	1.59	$-1.5 \times 10^{-23}$
polyisoprene (PI)	1.52	$1.0 \times 10^{-23}$
polybutadiene (PB)	1.52	$(3-9) \times 10^{-24}$
poly(2-vinylpyridine) (P2VP)	1.62	$-1.5 \times 10^{-23}$
poly(methyl methacrylate) (PMMA)	1.49	$1.6 \times 10^{-24}$
poly(ethylene-propylene) (PEP)	1.48	$4 \times 10^{-24}$
poly(ethylethylene) (PEE)	1.487	$4 \times 10^{-24}$
block copolymer	$\Delta n_f \times 10^3$	$\Delta n_i \times 10^3$
PS-PI	-1.6	-0.5
PS-PB	-1.6	-1 to -0.5
PS-P2VP	-0.28	-2.7
PS-PMMA	-3.2	-1.2
PEP-PEE	-0.017	0.7
		$\Delta n_i / \Delta n_f$
		-40

reasonably consistent with the data. Chin et al. also discuss the possibility that deformation birefringence plays a role for their samples, wherein the annealing of a glassy sample in a confined geometry does not relax all significant distortions of bond angles, leading to an additional optical anisotropy. Such an hypothesis merits further attention.

Given the variety of different block copolymer samples currently available, it is of interest to estimate the relative intrinsic and form birefringence contributions for different pairs of monomers. Table II presents a summary of the results for lamellar block copolymers. Estimated values of *n* and  $\alpha_1 - \alpha_2$  are tabulated,<sup>31</sup> as are values of the form birefringence calculated via eq 44 for a volume fraction of 0.50. The intrinsic birefringence contribution depends on both *M* and  $L^2/\langle h^2 \rangle_0$ ; in Table II, the former has been assumed to be  $3 \times 10^4$  and the latter equal to unity, and all densities have been taken as 1 g/cm<sup>3</sup>. For the three block copolymers with large differences in refractive index, namely, PS-PI, PS-PB, and PS-PMMA, the ratio of the intrinsic to the form birefringence is about 1/3. For the two samples that are almost index-matched, PS-P2VP and PEP-PEE, the intrinsic contribution dominates. Thus, it is clear that to investigate the intrinsic birefringence of block copolymer microstructures, the latter two samples are to be preferred. As  $\Delta n_i$  is predicted to decrease with increasing *M*, in principle one may anticipate a crossover to a regime where  $\Delta n_f$  dominates completely at high *M*. However, most block copolymer samples fall in the range  $10^4 \leq M \leq 10^5$ , so that, in practice, this regime may not be attained.

## Summary

Expressions have been derived for the static intrinsic birefringence and dichroism of tethered, flexible chains and particularly for lamellar and cylindrical block copolymer microstructures. Both quantities are predicted to be directly proportional to the stretching of the individual chains, given by the ratio  $L^2/\langle h^2 \rangle_0$ . The average optical anisotropy of each chain has been calculated in the strong-stretching limit, using the classical trajectory approximation for the average chain conformation, for chains tethered to planar or concave surfaces. For a convex tethering surface, such as for block copolymers in a cylindrical microstructure, the classical trajectory analogy leads to an unphysical free-end distribution, so a  $\delta$  function approximation was adopted. In all cases, the results are not greatly different from those obtained with a uniform stretching assumption. Thus, one may anticipate that the predictions should be reasonable even for values of  $L^2/\langle h^2 \rangle_0$  near 1, where the chains may be considered to be oriented but not stretched. Conversely, if the average

anisotropy at various locations along the chain contour is considered, there is a substantial difference between the classical trajectory and the uniform stretching assumptions, a difference that should be experimentally observable via infrared dichroism. A variety of relevant experiments have been performed, particularly in terms of the static birefringence of block copolymer microstructures, but not a sufficient number to provide a quantitative assessment of the predictions given here.

**Acknowledgment.** This work was supported by the National Science Foundation, through Grant DMR-9018807 (T.P.L.), and Presidential Young Investigator Grant DMR-9057147 (G.H.F.). Helpful discussions with E. Helfand and N. Balsara, and the willingness of S. Hsu and T. Russell to provide preprints of their results prior to publication, are appreciated.

## References and Notes

- Halperin, A.; Tirrell, M.; Lodge, T. P. *Adv. Polym. Sci.* 1991, 100, 31.
- Alexander, S. *J. Phys. (Paris)* 1977, 38, 977. de Gennes, P.-G. *J. Phys. (Paris)* 1977, 37, 1443.
- Milner, S. T.; Witten, T. A.; Cates, M. E. *Europhys. Lett.* 1988, 5, 413. Milner, S. T.; Witten, T. A.; Cates, M. E. *Macromolecules* 1988, 21, 2610.
- Semenov, A. N. *Sov. Phys. JETP* 1985, 61, 733.
- Kuhn, W.; Grün, F. *Kolloid Z.* 1942, 101, 248.
- Folkes, M. J.; Keller, A. *Polymer* 1971, 12, 222.
- Folkes, M. J.; Keller, A. *J. Polym. Sci., Polym. Phys. Ed.* 1976, 14, 833, 847.
- Zimm, B. H. *J. Chem. Phys.* 1956, 24, 269.
- Born, M.; Wolf, E. *Principles of Optics*; Pergamon: New York, 1970.
- Helfand, E.; Wasserman, Z. R. *Macromolecules* 1976, 9, 879.
- Ball, R. C.; Marko, J. F.; Milner, S. T.; Witten, T. A. *Macromolecules* 1991, 24, 693.
- Man, V. F.; Schrag, J. L.; Lodge, T. P. *Macromolecules* 1991, 24, 3666.
- Lodge, T. P.; Amelar, S. *Rheol. Acta* 1992, 31, 32.
- Noda, I.; Smith, S. D.; Dowrey, A. E.; Grothaus, J. T.; Marcott, C. *Mater. Res. Soc. Symp. Proc.* 1990, 171, 117.
- Shull, K. R. *J. Chem. Phys.* 1991, 94, 5723. Shull, K. R.; Winey, K. I. Unpublished results.
- Stein, R. S. *J. Appl. Phys.* 1961, 32, 1280.
- Jasse, B.; Koenig, J. L. *J. Polym. Sci., Polym. Phys. Ed.* 1979, 17, 799. Faivre, J. P.; Xu, Z.; Halary, J. L.; Jasse, B.; Monnerie, L. *Polymer* 1987, 28, 1881.
- Cosgrove, T.; Heath, T.; van Lent, B.; Leermakers, F.; Scheutjens, J. *Macromolecules* 1987, 20, 1692.
- Murat, M.; Grest, G. S. *Macromolecules* 1989, 22, 4054.
- Chakrabarti, A.; Toral, R. *Macromolecules* 1990, 23, 2016.
- Murat, M.; Grest, G. S. *Macromolecules* 1991, 24, 704.
- Lai, P.-Y.; Binder, K. *J. Chem. Phys.* 1991, 95, 9288.
- Patel, S. S. In *Mathematics and Industrial Problems*; Friedman, A., Ed.; Springer-Verlag: Berlin, 1991; Part 4.
- Waldman, D. A.; Kolb, B. U.; McCarthy, T. J.; Hsu, S. L., preprint.
- Amundson, K.; Helfand, E.; Patel, S. S.; Quan, X.; Smith, S. D. *Macromolecules* 1992, 25, 1935.
- Balsara, N. P.; Perahia, D.; Safinya, C. R.; Tirrell, M.; Lodge, T. P. *Macromolecules* 1992, 25, 3896.
- Chin, I.; Smith, B. A.; Russell, T. P., unpublished results.
- Bates, F. S.; Fredrickson, G. H. *Annu. Rev. Phys. Chem.* 1990, 41, 525.
- Tsvetkov, V. N. *Sov. Phys. Usp.* 1964, 6, 639.
- Wiener, O. *Abh. Sacch. Ges. Akad. Wiss., Math.-Phys. Kl.* No. 6 1912, 32, 575.
- The refractive indices in Table II are representative values. The value for poly(ethylethylene) was estimated from that for poly(ethylene-propylene), using the difference in densities and the Lorentz-Lorenz equation. Values for  $(\alpha_1 - \alpha_2)$  were computed from typical values for the stress-optical coefficient, *C*, according to  $(\alpha_1 - \alpha_2) = 9CnkT/2\pi(n^2 + 2)^2$ .

**Registry No.** PS-PI (block copolymer), 105729-79-1; PS-PB (block copolymer), 106107-54-4; PS-P2VP, 108614-86-4; PS-PMMA (block copolymer), 106911-77-7; PEP-PEE (block copolymer), 119008-27-4.